Hindawi
Advances in Civil Engineering
Volume 2021, Article ID 6643643, 14 pages
https://doi.org/10.1155/2021/6643643

Research Article

Tensile Performance of SHCC Road-Bridge Link Slabs in Fully Jointless Bridges

Xuefang Zhan, Kaile Liu, Yi-Bin Zhao, and Hengli Yan

College of Civil Engineering, Central South University of Forestry and Technology, Changsha 410004, China

Correspondence should be addressed to Yi-Bin Zhao; janehnu@hotmail.com

Received 1 November 2020; Revised 14 December 2020; Accepted 16 January 2021; Published 31 January 2021

Academic Editor: Valeria Vignali

Deformation of the main girder is absorbed by a continuously reinforced concrete pavement (CRCP) with microcracks in fully jointless bridges. The conventional fully jointless bridge has been challenged by durability and reliability issues because the CRCP is vulnerable to crack and hard to control the crack width when it suffers temperature variation. In this paper, a new type of fully jointless bridge with the road-bridge link slabs using strain-hardening cementitious composite (SHCC) material is investigated. First, an experiment was carried out to study the material properties of SHCC material for a preliminary assessment of road-bridge link slab performance using this material. Results found that SHCC is adequate for link slabs for its high tensile ductility and fine cracks development. Second, an SHCC slab model tensile test was carried out to study the absorptive capacity and the crack distribution of the SHCC slab. Results verified the high absorptive deformation capacity of the SHCC slabs. When the longitudinal deformation reaches 10 mm, the surface cracks in the SHCC slab are fine and dense, the crack width is kept in 80 μm, and the internal force is small. Third, by comparing the tensile test results with a conventional CRCP slab with same length, it is found that an SHCC slab has higher absorption capacity, better crack distribution, and smaller internal force than a CRCP slab. Finally, through ABAQUS finite element modelling, the stress performance of SHCC road-bridge link slabs is simulated using a trilinear constitutive model. The calculated results are consistent with the experimental results.

1. Introduction

Expansion joints are one of the main causes of high maintenance costs in bridges. At present, there are two ways to solve the problem caused by bridge expansion joints [1]: one is to improve the expansion device and the second is to build jointless bridges. The bridge engineer Henry Derthick made it clear: "The only good joint is no joint," that is, to cancel the bridge expansion joint. At present, the corresponding bridge is called a "jointless bridge," which includes the following four types (Figure 1) [2]: (1) jointless deck bridges (JDBs) [3], suitable for long multispan beam bridges; (2) integral/semi-integral abutment bridges (IABs/SIABs) [4], suitable for small and medium-span bridges with single or a few spans; (3) single-joint semi-integral bridges (SJSBs) [5], suitable for large and medium-span bridges; and (4) fully jointless bridges (FJBs) [6, 7], suitable for small and medium-span bridges with a single span or a few spans.

In the 1990s, Jin et al. [6] put forward a fully jointless bridge, which is a bridge comprising continual bridge decks, road-bridge link slab (included the approach slab, continuously reinforced concrete pavement (CRCP)), and the anchored beam, which is symmetrical to the temperature centre as shown in Figure 1(d). This kind of bridges not only eliminates the deck joints but also eliminates the joints between the bridge and the approach road. Extensive studies have been conducted by Jin et al. [6] and Zhan et al. [7, 8] about their performance, and the results suggested that temperature is the main factor affecting the mechanical performance of the fully jointless bridge, especially suffering seasonal temperature decreases. The bridge deck and road-bridge link slab are rigidly connected in the fully jointless bridge. Once the seasonal temperature decreases, the bridge decks shortened and it pulls one end of road-bridge link slab to move to the centre of the bridge, but the other end anchored to the anchor beam, then road-bridge link slab is at

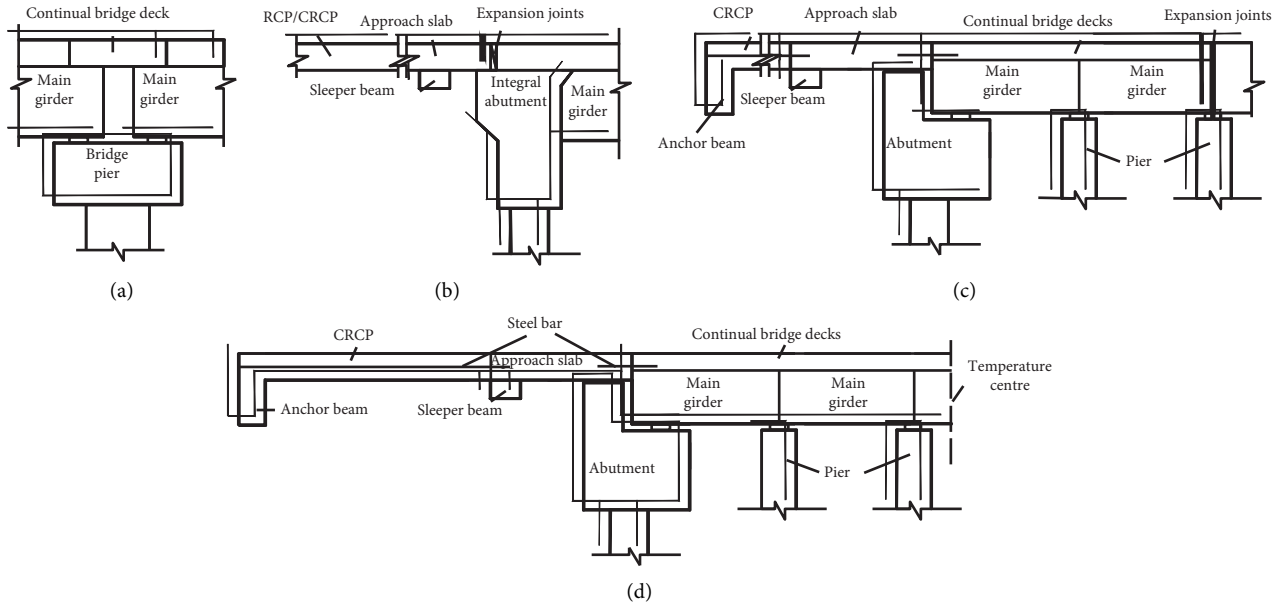

Figure 1: Structural types of jointless bridges: (a) JDBs, (b) IABs/SIABs, (c) SJSBs, and (d) FJBs.

an unfavorable tension state. Due to the limitation of material properties of the CRCP (Figure 1(d)) connected to the approach slab, it exhibits low stiffness and undergoes severe cracking. In particular, the crack width in the pavement increases and the durability decreases under repeated thermal and traffic load [7]. These years, many fully jointless bridges have been designed and built in Western China. Two of them were built in Yunnan Province (in China) in 2015 in which big cracks had been found on the CRCP in Feb 2019 under four years' repeated thermal and traffic load as shown in Figure 2. These cracks are below acceptable serviceability limit allowance.

Hence, for road-bridge link slab application, certain material properties must be satisfied: high strength for structural integrity; high tensile ductility to ensure serviceability and reliability under service traffic loads and temperature loads; and especially high absorption capacity for longitudinal deformation caused by temperature variety, shrinkage, and creep of concrete of the main girder.

Strain-hardening cementitious composite (SHCC) is a type material of unique ultra-high tensile ductility and tight crack width, which are exploited in application to improve bridge deck constructability, durability, and sustainability [9, 10]. Large-scale testing of SHCC link slabs was conducted by Kim et al. [11] to investigate the load capacity and fatigue performance of SHCC link slabs, along with the development of cracking on the SHCC link slab. Kim et al. found that SHCC material was a suitable choice for construction of link slabs. During monotonic loading, a lower stress in the reinforcement was found in SHCC link slabs and cycle tests revealed that crack width in the SHCC link slab remains less than 60 μm. Wheel abrasion studies were carried out by Li et al. [12, 13] on the SHCC slab, and they found it meets the minimum standards required by the State of Michigan. The other full-scale load test was conducted by Michael and Li [14] to explore the structural response of the constructed SHCC link slab. SHCC link slab is placed at the expansion joint to connect the bridge span of the simply supported beam. And the high strain capacity of SHCC is used for absorption of the longitudinal deformation due to temperature change as designed. Two years after this SHCC link slab was placed, the performance of this link slab remains unchanged. Li [15] suggested that SHCC was an application to construct a bridge deck link slab. Thus, the introduction of SHCC to road-bridge link slab construction is proposed for its ability to control crack widths and its successful use in link slabs.

Hence, an SHCC road-bridge link slab (Figure 3) is proposed to replace the traditional road-bridge link slab (Figure 1(d)), which makes the transmission path of force from the main girder to approach pavement much simpler.

The purpose of this paper is to demonstrate the tensile performance of road-bridge link slabs designed with SHCC material for a macroscopically crack-free jointless bridge. First, based on the consideration of the cost of the material and needed absorption deformation, in this paper, the tensile properties of SHCC material will be studied and a better mix design has to be found. The goal of the experiment was to obtain a hands-on experiment on mix design and propose recommended mix design for further SHCC road-bridge link slab construct. Second, when temperature decreases, the SHCC road-bridge link slab is at an unfavorable tension state. As mentioned earlier, temperature load can be expressed by equivalent tensile longitudinal deformation. Then, the lab test of the tensile performance of SHCC road-bridge link slabs will be carried out. The test results will be compared with those of a conventional road-bridge link slab constructed of reinforced concrete. The absorption deformation capacity, crack distribution, and slab deformation associated with the development of slab stress and crack

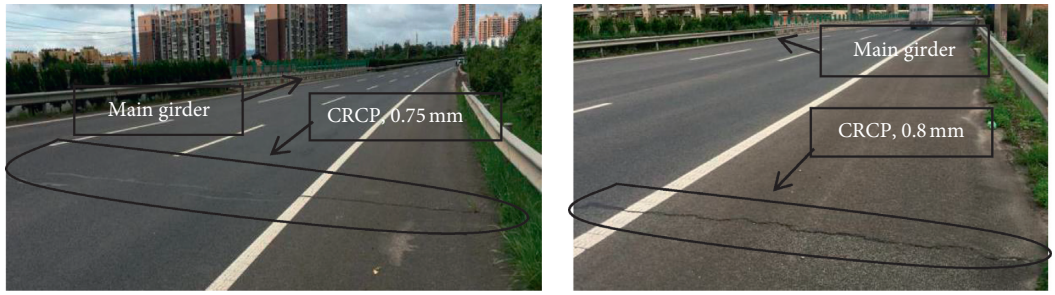

(a) (b)

Figure 2: Photos of cracks in CRCP during service of fully jointless bridge: (a) Lihecun fully jointless bridge (in Feb 2019) and (b) Xinrong No.1 fully jointless bridge (in Feb 2019).

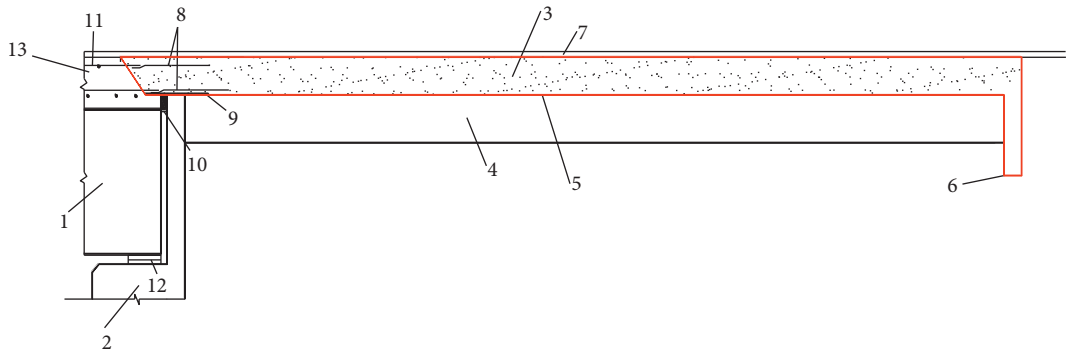

Figure 3: Diagram of the SHCC road-bridge link slab. (1) Main girder; (2) abutment; (3) SHCC slab; (4) concrete base; (5) emulsified asphalt layer (sliding layer); (6) anchor beam; (7) asphalt surface; (8) connect steel bar pavement slab; (9) synthetic pressure pad; (10) self-adhesive compressible sealing materials; (11) reinforcement in beams; (12) bearing; (13) bridge deck.

width will be discussed. The goal of the experiment was to prove the feasibility of SHCC material to make the SHCC road-bridge link slab.

2. SHCC Materials

2.1. SHCC Material Properties. SHCC is a kind of fine aggregate, including cement, sand, fly ash, fibre, water reducing agent, and so on. The volume fibre content of SHCC is about 2%, the fabrication process is flexible, its compressive strength is similar to concrete, but the compressive elastic modulus is lower than that of normal concrete [16, 17]. In the early 1990s, it was proposed by Li [16] through optimization of fibre, interface, and matrix based on the theory of micromechanics. Shortly, it was widely used in the United States, Japan, China, and other countries. The main performance indices of the SHCC are compared with the normal concrete (NC), as shown in Table 1.

2.2. SHCC Material Test. To gain a better understanding on material properties of SHCC material, a tensile performance test was conducted, and the tensile specimen model of SHCC material is shown in Figure 4. According to SHCC tensile research results [17], two groups of SHCC specimens with different mix designs are presented in Table 2.

The stress-strain relationships of axial tensile of SHCC test specimens with different mix designs are shown in Figure 5.

The experimental results show that the tensile stress at the formation of the initial crack in Specimen 1 is close to 2 MPa, the ultimate tensile strength is about 3.5 MPa, the corresponding tensile strain is 2.5%, and the ultimate tensile strain of the material is close to 4.3%. The tensile stress at initial cracking and ultimate state of Specimen 2 is close to 3.0 MPa, and the ultimate tensile strain reaches 0.825%. To reduce the internal force of the SHCC road-bridge link slab and provide a large tensile deformation capacity, the mix design of Specimen 1 is recommended for SHCC road-bridge link slab construction.

3. SHCC Road-Bridge Link Slab Tensile Test

3.1. Objective and Overview. Under the temperature load, the main girder pulls/pushes SHCC road-bridge link slabs working together. As we know, the stiffness of the main girder is bigger than the SHCC road-bridge link slab. When the temperature decreases, the SHCC road-bridge link slab is in tension, and the bridge decks shorten and move to the temperature centre of the bridge with the link slab. If the tensile stress exceeds the initial crack stress of the SHCC slab, it ensues cracking. The number of cracks increases with the increase of longitudinal deformation towards the temperature

Table 1: Main performance index comparison between SHCC and NC [16].

Type of concrete	SHCC	NC	SHCC/NC
Compressive strength (MPa)	20–95	20–50	1
Tensile strength of initial crack (MPa)	2–7	—	—
Ultimate tensile strength (MPa)	3.5–12	1.2–3.1	3
Extreme tensile strain (%)	1–5	0.01–0.015	100
Elastic modulus (GPa)	18–34	30–40	0.6
Flexural strength (MPa)	10–30	2–5	5
Chloride diffusion coefficient (m^2/s)	0.1×10^{-12}	1.1×10^{-12}	1/10

(a)

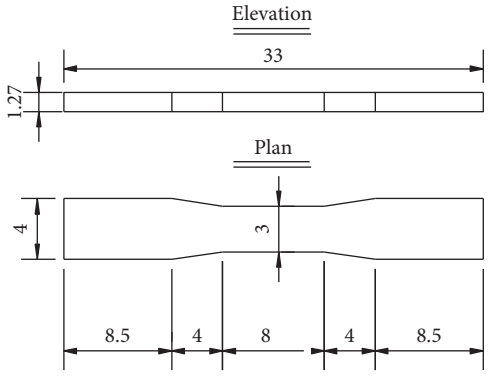

(b)

Figure 4: Tensile experiment of SHCC specimens (cm): (a) tensile experiment and (b) SHCC specimens.

Table 2: Material mix designs of SHCC (kg/m^3).

Category	Cement	Fly ash	Sand	Maximum sand size	Water	PVA fibre (vol%)	Water reducing agent
1	550	650	550	0.3	395	2	12.8
2	530	530	530	1.18	424	2	12.8

centre of the bridge. It is not easy to measure the tensile stresses translated from the main girder to SHCC road-bridge link slab when the seasonal temperature decreases. Nevertheless, the longitudinal deformation caused by temperature variety, shrinkage, and creep of concrete of the main girder can be calculated as follows:

$$\Delta l = \Delta l_T + \Delta l_{SC} + \Delta l_O, \quad (1)$$

where Δl represents the total longitudinal deformation; Δl_T represents the longitudinal deformation caused by temperature variety; Δl_{SC} represents the longitudinal deformation caused by concrete shrinkage and creep of the main girder; and Δl_O represents the longitudinal deformation caused by other factors.

The longitudinal deformation Δl_T caused by temperature variety can be calculated straightforwardly as follows:

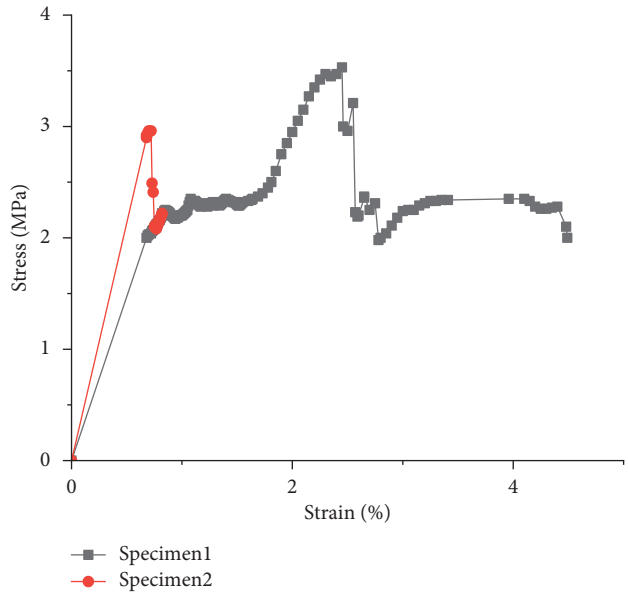

Figure 5: Stress-strain relationship of the SHCC specimen.

$$\Delta l_T = \alpha \cdot \Delta T \cdot L, \tag{2}$$

where α represents the thermal expansion coefficient, $\alpha = 1 \times 10^{-5}$ for concrete; ΔT represents the temperature variety; and L represents the temperature length.

Once the SHCC road-bridge link slab cracks, its serviceability and reliability are affected. It is not easy to simulate the effect of temperature load in the laboratory, but SHCC road-bridge link slabs suffering temperature decreases can be replaced by equivalent longitudinal deformation calculated according to the formula (2). To gain a better understanding on the applicability and deformation performance of the SHCC road-bridge link slab, when it is in the most unfavourable condition suffering the temperature drops, the tensile simulation test of the SHCC slab was conducted in the lab. The goal of the experiment was to prove the feasibility of SHCC material to make the SHCC road-bridge link slab.

Nevertheless, before this, another test is required. In a jointless bridge, axial tension produced by main girder contraction is mainly offset by friction between the SHCC road-bridge link slab and concrete base. The CRCP of traditional fully jointless bridge used to absorb the longitudinal deformation is always set at an extended length of about 20 ~ 30 m. However, for the high cost of SHCC material, the SHCC road-bridge link slab is generally provided with a length from 5 m to 10 m. If a larger coefficient of friction is set between two layers, the stress in the SHCC slab being enormous, the stress transfer to the anchor beam remains small; if the coefficient of friction is small, the stress in the SHCC slab being small, the stress transfer to the anchor beam is massive. Therefore, a suitable interlayer coefficient of friction has an essential effect on the economy and durability of such jointless bridges. Hence, the coefficient of friction needs to be measured before the tensile performance test of the SHCC slab.

3.2. Lab Test

3.2.1. Model Design. The test model built-in lab is a $5.5 \times 0.5 \times 0.15$ m SHCC slab. Both ends of the slab are provided with tension and anchor. To ensure the cracks appeared on the SHCC slab, the sizes of the two ends are enlarged, as shown in Figures 6(a) and 6(b). The SHCC slab reinforced with 3 Φ16 12 mm bars. The slab was cast-in-place on a C10 concrete base with a length of 7 m, a width of 0.5 m, and a height of 0.3 m. An emulsified asphalt sealing layer worked as a slipping layer of 2 mm in thickness lays between the SHCC slab and the concrete base, as shown in Figure 6(c).

3.2.2. Material Parameters. Basic material parameters of the SHCC slab are summarized in Table 3.

3.2.3. Layout of Measuring Instrument. Two pressure gauges (P1 and P2) were arranged at the tension ends to measure the tensile force, and the other two pressure gauges (P3 and P4) were arranged at the anchor ends to measure the force translated from the tension ends, as shown in Figures 6(b) and 6(f).

Ten dial gauges used as displacement gauges (from D1 to D10) shown in Figure 6(b) were arranged on the slab, and two dial gauges (D1 and D2) were added to the tension end to measure the total longitudinal displacement (the tension control displacement). Eight dial gauges (D3 ~ D10) were arranged on each side of the slab to measure the displacement at different distances, as shown in Figures 6(b) and 6(g). The distances of measure points (No. 1 ~ No. 5) away from the tension end are 1 m, 2 m, 3.5 m, and 5.5 m, respectively.

Two strain gauges (S1 and S2) were bound to the steel bar to measure the strain of the steel bar. Strain gauge S1 was arranged at the tension ends and S2 was arranged at 2.5 m away from the tension ends, as shown in Figures 6(b) and 6(h).

3.2.4. Test Programme. As mentioned earlier, there are two tests that need to be performed. Test 1 is to measure the interlayer coefficient of friction of the emulsified asphalt sealing layer. By pushing the SHCC slab with two 100-t jacks in one direction at the tension end to move on the concrete slab. A force in 5 tons increments is applied until the SHCC slab is detached from the emulsified asphalt layer. Experiment results and figures of the test were stored for results analysis as shown in Figure 7 and Table 4.

Test 2 is to test the tensile performance of the SHCC slab. Here, we simulated a 100 m fully jointless bridge suffering 20°C temperature decreases, and the temperature centre is near, or at the centre of the bridge, and then the longitudinal deformation can be calculated using formula (2): $\Delta l_T = 1 \times 10^{-5} \cdot 20 \cdot (100\,\text{m}/2) = 10\,\text{mm}$. Thus, the controlled longitudinal displacement is 10 mm. By loading at the loading end of the SHCC slab with two jacks in the same direction, as shown in Figure 7(a) to simulate the

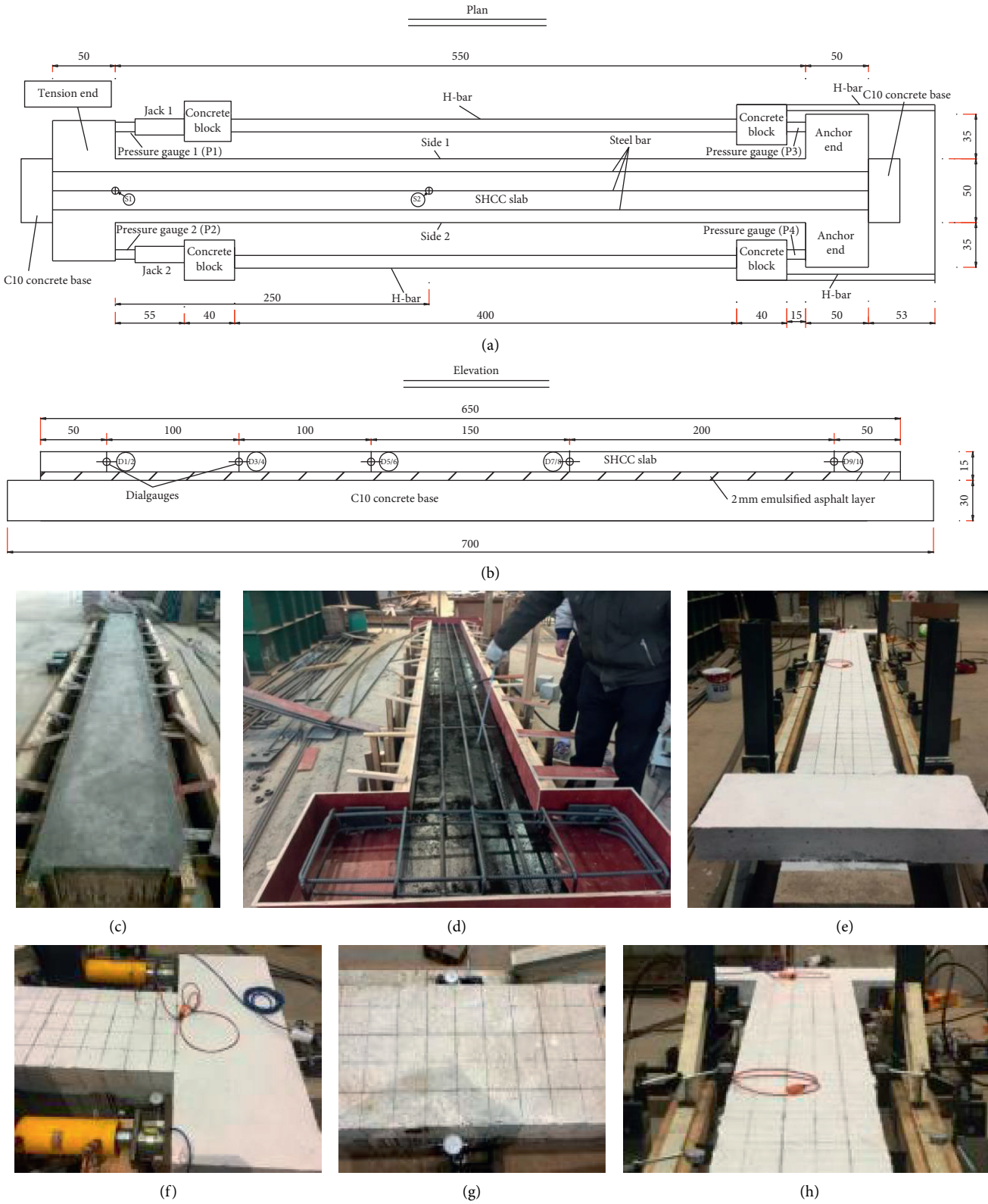

Figure 6: Illustration of the SHCC slab experimental model (unit: cm). (a) Model plan. (b) Model Elevation. (c) C10 concrete base, (d) Laying of the emulsified asphalt sealing layer. (e) Test model. (f) Load diagram. (g) Dial gauges. (h) Strain gauges.

longitudinal deformation of the main girder, the displacement is controlled by the tension displacement of the SHCC slab. Loading displacement is applied in 1 mm increment until the full extension reaches 10 mm. Experiment results and figures of the test were stored for results analysis as shown in Figure 8(a) and Table 5.

Table 3: Experimental model parameters.

Numbers of longitudinal reinforced bars of SHCC slab	The diameter of the longitudinal steel bar (mm)	Longitudinal reinforcement ratio of SHCC slab (%)	Tensile strength of steel bar (MPa)	Tensile strength of SHCC (MPa)	SHCC slab density (kg/m^3)	SHCC elasticity modulus (MPa)
3	12	0.452	335	3.5	21.8	1.8×10^4

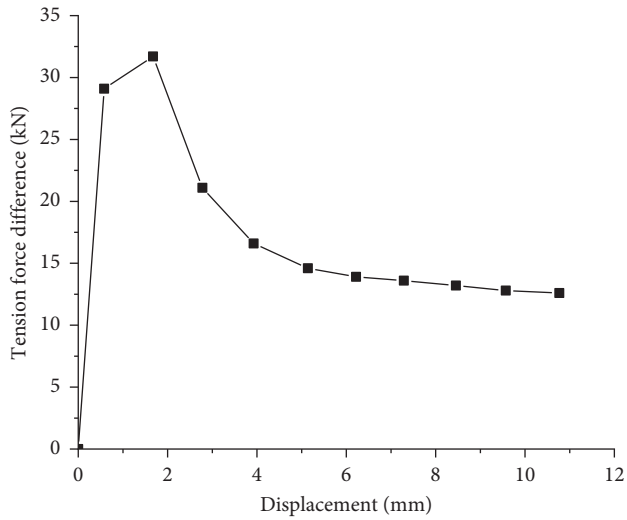

Figure 7: Relationship between tension difference and longitudinal displacement.

Table 4: Measured coefficients between SHCC slab and concrete base.

Type of seal layer	Cohesion coefficient	Sliding friction coefficient
Emulsified asphalt	2.4	1.05

4. Results Analysis

4.1. Test 1. The coefficient of friction is calculated by dividing the measured force difference between the tension end and the anchor end by gravity. The calculated relationship between tension difference and longitudinal displacement is shown in Figure 7.

Figure 8(b) shows that the force difference between the two ends was 31.7 kN when the slab detached from the emulsified asphalt layer. Once the SHCC slab slides on the concrete base, the force difference between the two ends is around 13.6 kN. The gravity of the SHCC slab is known as 13 kN, so the interlayer coefficients can be calculated as shown in Table 4.

4.2. Test 2. A 10-cycle load trial was conducted on this SHCC slab model as a tensile test. During the whole experiment, the total longitudinal displacement of the SHCC slab was 10 mm. The absorption deformation capacity, internal force, and crack distribution of the SHCC slab have been analyzed, as well as the anchoring force of the anchor beam.

4.2.1. Absorption Deformation Capacity of the SHCC Slab. The tensile test of the SHCC slab was controlled by the longitudinal displacement. Once the longitudinal displacement increases, the tension force increases. When the force reaches 10 tons, the first crack appeared on the surface of the SHCC slab. The quantities of the cracks increased with the increase in longitudinal displacement; however, the crack width was generally within 80 μm. When the displacement reached 10 mm, the absorption rate reached $\delta = 10\,\text{mm}/5.5\,\text{m} = 0.18\%$, far less than the strain capacity of SHCC material (1% ~ 5%). The results proved that the SHCC slab has a high absorption capacity of the longitudinal displacement, and the structure is in great integrity.

4.2.2. Internal Forces of the SHCC Slab. Due to the friction under the SHCC slab, the tensile stress near the SHCC end is higher than the tensile stress near the end of the anchor beam (Figure 9). When the longitudinal tensile displacement of the SHCC slab reaches 10 mm, the maximum tension force at the tension end reaches 210.2 kN. The cross-sectional area of the SHCC slab AC is known to be $\text{AC} = 0.15\,m \times 0.5\,m = 0.075\,\text{m}^2$, and then the stress on the SHCC slab can be calculated as $\sigma_{b1} = 2.8\,\text{MPa} < 3.5\,\text{MPa}$ (SHCC ultimate tensile strength). Given the elastic modulus of the SHCC slab of 18 GPa (Table 4), the strain in the SHCC slab can be calculated as 156 $\mu\varepsilon$. Meantime, the strain in the steel bar in the SHCC slab was measured at 162 $\mu\varepsilon$, and then the tensile stress on the steel bar can be calculated to be 32.4 MPa. The strain difference between the steel bar and SHCC slab is minimal, which indicates that the steel bar and SHCC slab participate together, and the microcracks of the SHCC slab do not affect its performance.

4.2.3. Longitudinal Displacement. The displacement curves of five displacement measuring points (Figure 5(b)) of the SHCC slab with loading displacement are drawn (Figure 10). From the curve, it can be found that the displacement of the SHCC slab changes linearly, so the stress distribution of the SHCC slab is uniform, which verifies the assumption that the base friction stress is uniformly distributed.

4.2.4. Crack Width. When the tensile stress (σ_{bi}) at any crack section i (Figure 9) of the SHCC slab is greater than the initial crack strength (f_t) of the road-bridge link slab, then a crack appeared in that section, but the crack width is smaller than 80 μm. As the deformation of the beam increases, the tensile stress increases, also the number of cracks in the SHCC slab increases, but the crack spacing (l_m) decreases. Where σ_{bi} is less than its ultimate tensile strength ($\sigma_{bi} < f_{tu}$),

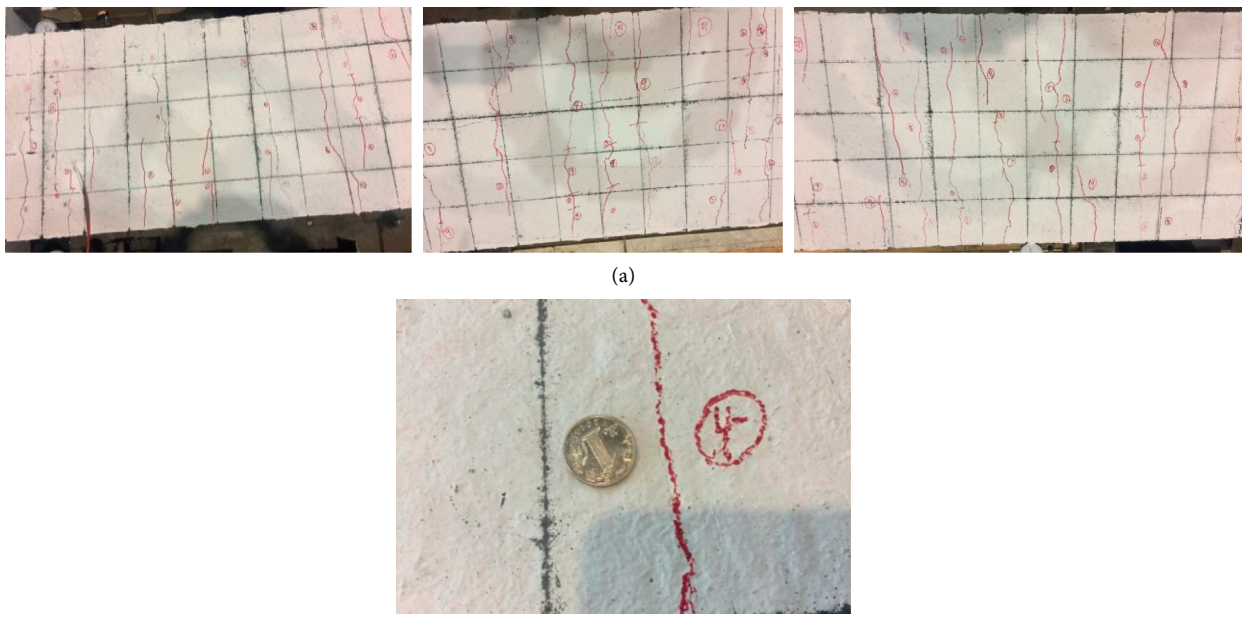

(a)

(b)

Figure 8: Cracking pattern of the experimental model (unit: cm). (a) Distribution of local cracks in the SHCC slab. (b) SHCC slab crack width diagram.

Table 5: Comparison of crack width and crack spacing: experimental and theoretical values.

Types	Numbers of cracks (n)	Average crack width (μm)	Maximum crack width (μm)	Minimum crack width (μm)	Average crack spacing (cm)	Maximum crack distance (cm)	Minimum crack distance (cm)
Measured value	154	65	80	40	3.6	10	2
Theoretical value	≥125		80		4.4		

the width of the crack remains constant until absorbing all deformation of the main girder. Conversely, if $\sigma_{bi} \geq f_{tu}$, the width of the crack will increase sharply, until the PVA fibre is pulled out or broken to form a big joint, thus generating structural damage. So, the crack width w_i at any crack section i can be calculated as follows:

$$\begin{aligned} w_i &\leq 80\,\mu\text{m}, \quad \text{if } f_I \leq \sigma_{bi} < f_t, \\ w_i &= w_{PVAi}, \quad \text{if } \sigma_{bi} \geq f_t, \end{aligned} \tag{3}$$

where w_{PVAi} represents the tensile deformation of the fibre or the pull-out length of a PVA fibre at any crack section i before fracture.

Therefore, to ensure the durability of the structure, we need to control the crack width of the SHCC slab by controlling the stress of the SHCC slab. Then, $\sigma_{bi} < f_{tu}$ ensures that the fibres are not pulled out or broken. Meanwhile, the stress σ_{PVAi} of the PVA fibre should be less than the pull-out stress of the fibre ($\sigma_{\text{PVApull out}}$): $\sigma_{PVAi} \leq \sigma_{\text{PVA}_{\text{pullout}}}$, also the stress σ_{PVA} shall be less than the fibre fracture stress ($\sigma_{\text{PVAfracture}}$): $\sigma_{PVAi} \leq \sigma_{\text{PVA}_{\text{fracture}}}$.

In this experiment, the calculated stress on the SHCC slab is $\sigma_{bI} = 2.8$ MPa < 3.5 MPa (SHCC ultimate tensile strength), then the crack width can be controlled within 80 μm, and the durability of the structure can be ensured.

4.2.5. Crack Spacing. If the length of the SHCC slab is L, the demand to absorb longitudinal deformation of the main girder is l, and if the crack width after the SHCC slab absorbed the main girder deformation is less, and the cracks are dense, then we can calculate the minimum number n of cracks that are needed to absorb longitudinal deformation l:

$$n \geq \frac{l}{80\,\mu\text{m}}. \tag{4}$$

Then, the average spacing l_m between adjacent cracks is calculated as follows:

$$l_m = \frac{L}{n}. \tag{5}$$

The 5.5 m-long SHCC slab is used to absorb 10 mm of longitudinal deformation, millions of dense cracks are found on the surface of the SHCC slab, and the crack width is within 80 μm; the minimum numbers of cracks can be calculated using formulae (4) and (5). When SHCC slab absorbing 10 mm longitudinal deformation, the minimum cracking can be calculated $n = 10$ mm/80 μm $= 125$; average crack spacing $l_m = 5.5$ m/125 $= 0.044\,m = 4.4$ cm (Table 5).

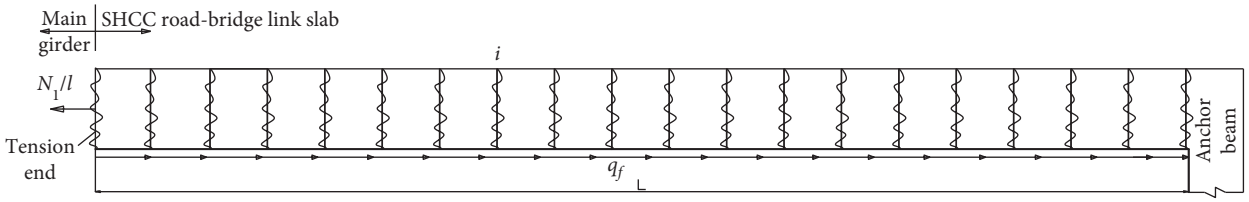

Figure 9: Stress diagram of SHCC when temperature decreases.

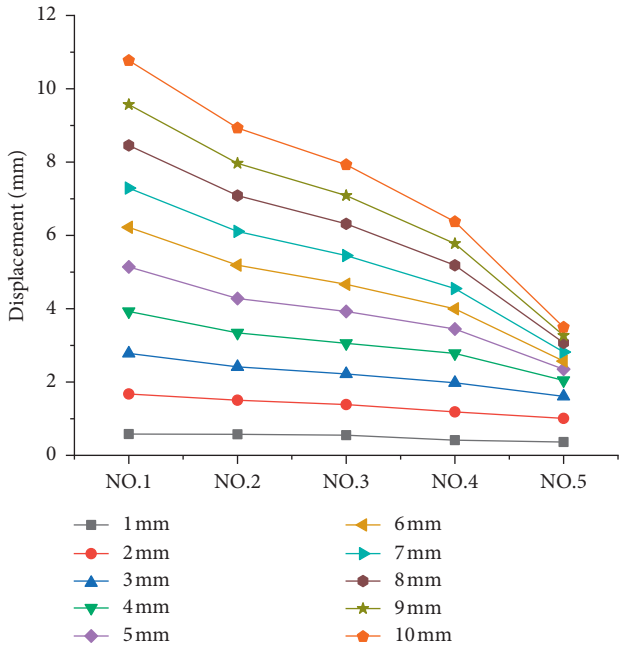

Figure 10: Displacement variation of displacement measuring point (No. 1 ~ No. 5).

It can be seen from Table 6 that the measured value is close to the theoretical value. After unloading, cracks on the SHCC slab model closed, no apparent bond failure was found, and no PVA fibres were pulled out.

4.2.6. Anchor Force of the SHCC Anchor Beam. The whole SHCC slab is intact after the tension, only small dense cracks developed, and the stress distribution at the bottom of the slab is uniform. When the longitudinal tensile displacement of the SHCC slab reaches 10 mm, anchor force on the anchor beam $N_d = 210.2\,\text{kN} - 1.05 \times 13\,\text{kN} = 196.6\,\text{kN}$ (close to the 200.2 kN measured). The results further demonstrate the integrity of the SHCC slab, but from another perspective, new design requirements are imposed upon the SHCC slab anchor beam for this high anchor force.

4.3. Results Compared with CRCP Slab [18]. In 2009, a CRCP slab (Figure 11) with the same length of 5.5 m was designed and the tensile test was carried out into simulating the temperature effect by Shao et al. [18]. Also, the comparison of absorption deformation capacity, crack distribution, internal force, and anchored force between CRCP slab and SHCC slab will be discussed.

Table 6: Comparison of absorption deformation capacity between CRCP slab [18] and SHCC slab.

	Absorb deformation (mm)	Tensile rate (%)
CRCP slab	6.5	0.12
SHCC slab	10	0.18

4.3.1. Comparison of Absorption Deformation Capacity. According to the ASSHTO, the maximum crack width of CRCP should be smaller than 0.8 mm for ensuring the durability of the CRCP and yield strength of reinforced bar should be less than 335 MPa for HRB335(steel bar used in China). Then, the CRCP slab only can absorb 6.5 mm longitudinal deformation, and the corresponding tensile rate is 0.12% [18]. However, the tensile rate of SHCC slab is 0.18%, which is far less than the general tensile rate (from 1% to 5%) of SHCC material. Compared with the test results (Table 6), it is found that the SHCC slab with the same length has a stronger ability to absorb deformation.

4.3.2. Comparison of Crack Distribution. In order to better control the crack distribution of CRCP slab, a precut joint is set every 1.2 m in the CRCP slab before the test, and four precut joints are found in a 5.5 m long slab, as shown in Figure 11(a). The precut joint is formed by burying a 2 mm plywood before pouring concrete, as shown in Figure 11(e). When the longitudinal tensile displacement reaches 6.5 mm, the crack width of four precut joints is different, as shown in Figure 12. The comparison results of measured crack width and spacing between the CRCP and SHCC slab are shown in Table 7 and Figure 12.

4.3.3. Comparison Internal Force. When the maximum longitudinal displacement of the CRCP slab reaches 6.5 mm, the stress of the steel bar at the tension end is 303 MPa [18]. Compared with the CRCP slab, the internal force of the SHCC slab is smaller when it absorbing more significant longitudinal deformation, which is more favorable for the structure. Comparison results are shown in Table 8.

4.3.4. Comparison of Anchor Force. With the increase of absorbing longitudinal deformation, the tensile force of CRCP slab transferred to the anchor end through the friction between CRCP slab and concrete slab. When the maximum longitudinal displacement of the CRCP slab reaches 6.5 mm, eight cracks were found in the CRCP slab (Figure 11(a)). Then the tension force at the tension end is 550 kN, and the anchored force is 504 kN [18]. Smaller anchor force was

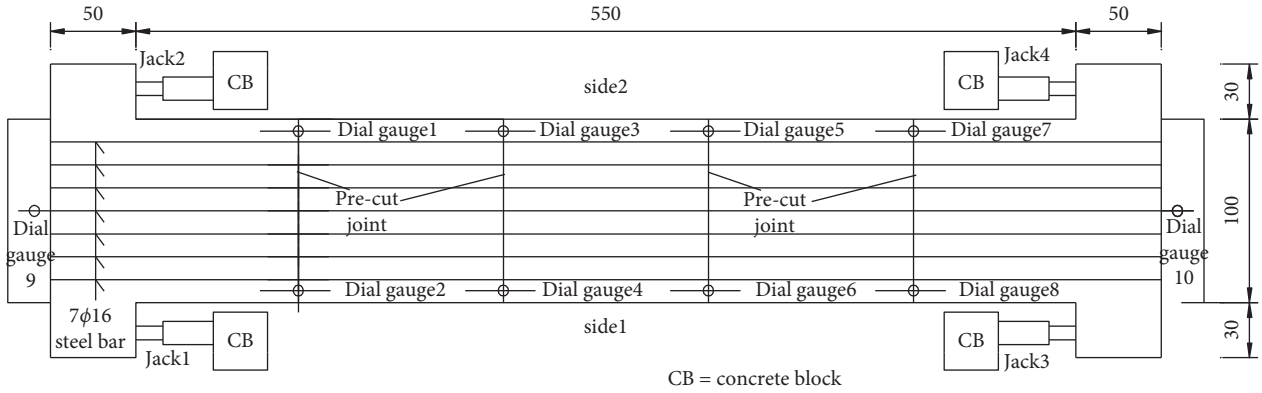

(a)

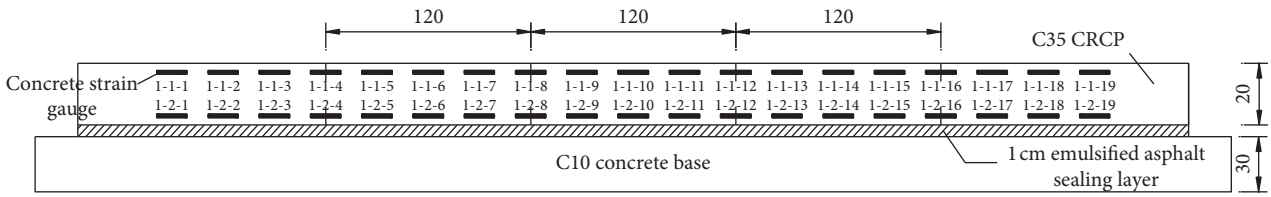

(b)

(c)

(d)

(e)

Figure 11: Illustration of the CRCP slab experimental model (unit: cm) [18]. (a) Plan. (b) Elevation. (c) Laying of the emulsified asphalt sealing layer. (d) Test model. (e) Plywood for precut joint.

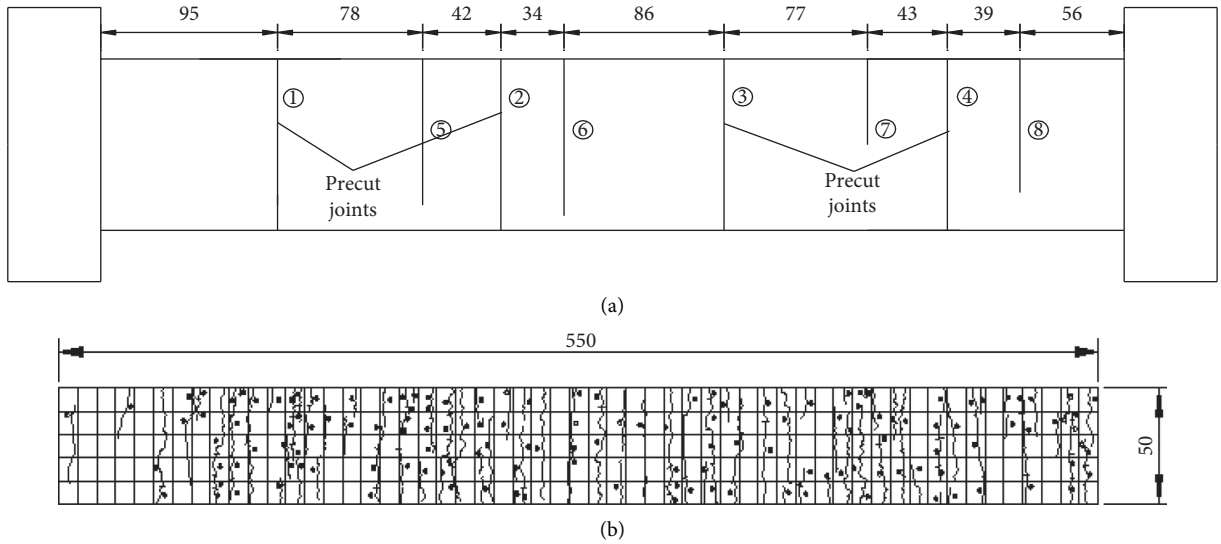

Figure 12: Comparison of crack distribution between CRCP slab and SHCC slab (unit: cm). (a) Crack distribution of CRCP slab [18]. (b) Crack distribution of SHCC slab.

Table 7: Comparison of measured crack width and spacing between CRCP slab [18] and SHCC slab.

Type	Numbers of crack n	Average crack width (μm)	Maximum crack width (μm)	Minimum crack width (μm)	Average crack spacing (m)	Maximum crack spacing (m)	Minimum crack spacing (m)
CRCP slab	8	456	787	194	0.61	0.86	0.34
SHCC slab	154	65	80	40	0.36	0.1	0.02

Table 8: Comparison of internal force between CRCP slab [18] and SHCC slab.

Types	Strain of slab ($\mu\varepsilon$)	Stress of slab (MPa)	Strain of steel bar at tension end ($\mu\varepsilon$)	Stress of steel bar at tension end (MPa)
CRCP slab	70	—	1471	303
SHCC slab	152	2.8	162	32.4

found in the SHCC slab. Comparison results are shown in Table 9.

Compared with the measured internal forces of tension end and anchor end, it is found that the internal force transferred to the anchor end of CRCP slab and SHCC slab is relatively large due to the small friction resistance and the limited set length of the model (5.5 m). Considering this situation, the set length of CRCP slab of the jointless bridge is relatively long about 20 m~30 m. However, due to the high cost, the SHCC is always with a short setting length of about 5 m–10 m, and then the anchor force transferred from the tensile end is considerable. Hence, it is necessary to design a larger anchor end or improve the friction distribution between SHCC slab and concrete base to optimize its stress state.

In conclusion, according to the comparison results, the SHCC slab has higher absorption capacity, better crack distribution, and smaller internal force than the CRCP slab, which supported that the SHCC slab is more suitable for the construction of a fully jointless bridge.

5. Numerical Analysis

5.1. Model Specifications. To compare the analysis results, ABAQUS software is used to simulate the tension process of the SHCC slab. Using a separating model to model the SHCC slab and base concrete separately, the SHCC slab and concrete base are simulated by C3D8R solid unit elements. The steel bar inside the SHCC slab is simulated by T3D2 truss elements. For a more accurate simulation of the SHCC slab and improvement of calculation accuracy, a finer mesh subdivision is used for the steel bar and the SHCC slab element (Figure 13).

Contact between steel bar and SHCC plate is subject to consolidation, without considering the effect of slipping of

Table 9: Comparison of anchor forces between CRCP slab [18] and SHCC slab.

Types	Tension force (kN)	Anchored force (kN)	Tension force Difference (kN)	Tension force difference/tension force (%)
CRCP slab	550	504	46	8.4
SHCC slab	210.2	196.6	13.6	6.5

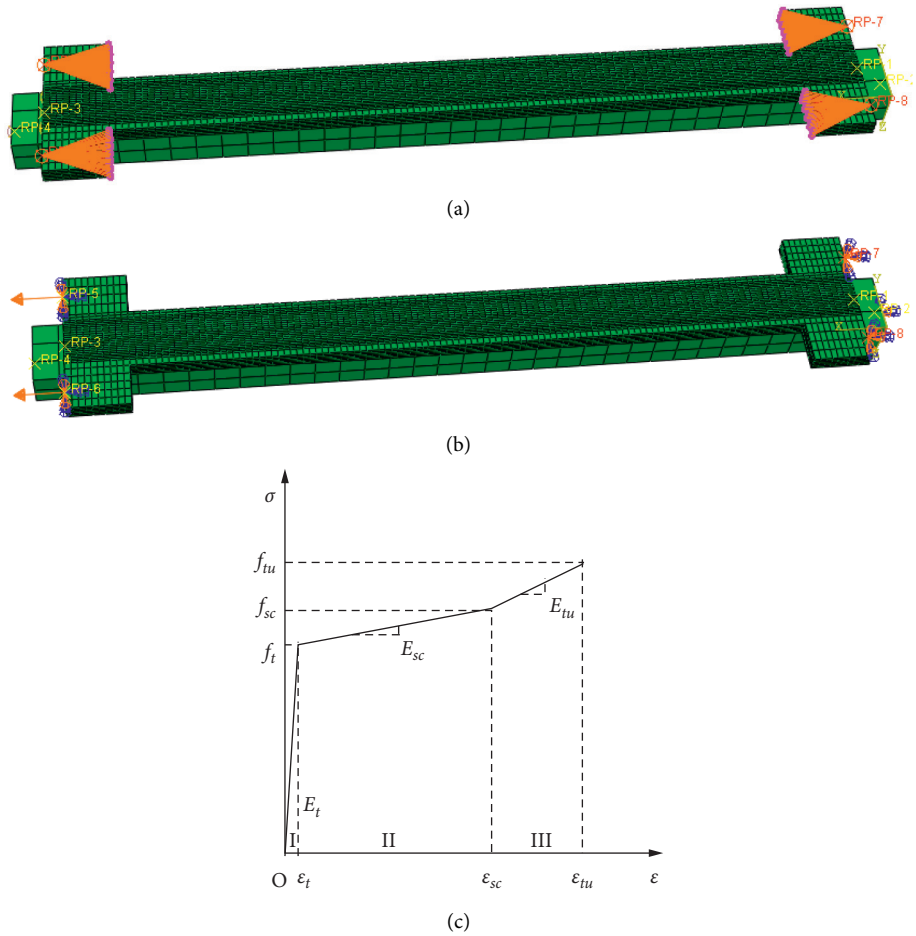

Figure 13: ABAQUS model of SHCC slab. (a) Grid division and constraints: the SHCC slab. (b) SHCC slab loading simulation. (c) Trilinear constitutive model. f_t (tensile initial crack strength) = 2.0 MPa, ε_t (tensile initial strain) = 0.0065, f_{sc}(corresponding stress in fracture saturation) = 2.35 MPa, ε_{sc} (corresponding strain in fracture saturation) = 0.0164, f_{tu}(extreme tensile strength) = 3.528 MPa, and ε_{tu} (extreme tensile strain) = 0.02455.

the steel bar. The constraint on the SHCC slab is RP5, RP6, RP7, and RP8, as shown in Figure 10. The model is loaded by displacement.

At present, two simplified models of the tensile stress-strain curve were proposed for SHCC material, that is the bilinear model recommended by Mohamed and Li [19] and trilinear model recommended by Li and Wu [20]. Here used a trilinear model (Figure 13(c)) which built by combining with the previous SHCC material test results (as shown in Figure 5).

5.2. Comparison of Finite Element Calculation and Experimental Results. As can be seen from Figure 14, the variation of the load-displacement curve of finite element analysis is basically consistent with the measured value. However, the results of finite element analysis are slightly higher than those obtained experimentally: this may have been because the finite element model is an ideal material model, and slippage of the steel bar is not considered in this comparison. The results show that the SHCC trilinear constitutive model can be safely used to simulate the tensile properties of an SHCC slab.

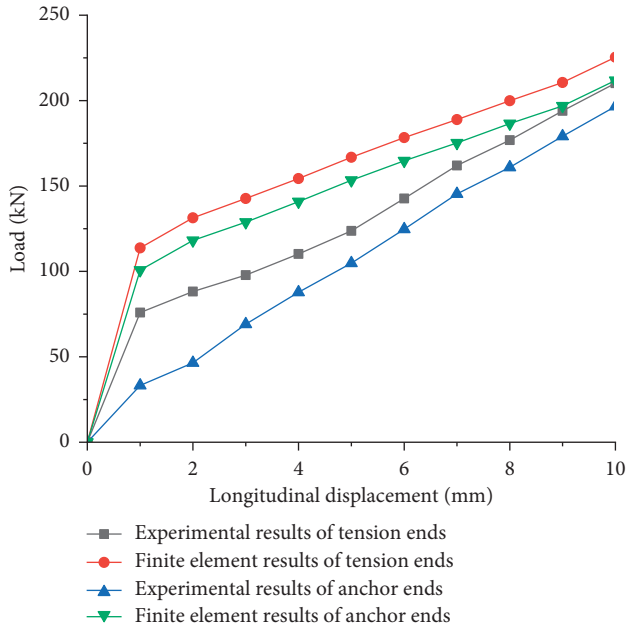

Figure 14: Comparison of experimental and finite element results.

6. Conclusions

Temperature is an essential factor that affects the mechanical performance of the fully jointless bridge. Meantime, vehicle load, uneven settlement behind the abutment, and other factors also affect its mechanical performance. Because of the length of the paper, this paper only studies the influence of seasonal temperature drop on the mechanical performance of the SHCC road-bridge link slab for the jointless bridge. Through the tensile test of the SHCC material and an SHCC slab, a tensile performance comparison between SHCC slab and CRCP slab, and the tensile numerical simulation of the SHCC slab, the following conclusions can be obtained:

(1) Through the tensile test of two groups of specimens, it is found that the SHCC material has strong ductility (the ultimate tensile strain is 4.5%) and fully meets the needs of jointless bridges. Also, the suitable SHCC material mix proportion for the SHCC road-bridge link slab is obtained, which provides design parameters for the configuration of the SHCC road-bridge link slab.

(2) Through the 10 mm longitudinal tensile test of a 5.5 m-long SHCC slab, it is found that the SHCC slab has a strong ability to absorb longitudinal deformation. When the SHCC slab is in tension, the surface of the slab develops many dense cracks; the crack width is within 80 μm, and the stress in the slab is small. Then, the feasibility of using SHCC to cast the road-bridge link slab of the jointless bridge is verified. However, because the large anchor force transferred to the anchor beam when the SHCC slab is in tension, it is necessary to give special consideration to the design of anchor end.

(3) By comparing the tensile performance with CRCP slab, it is found that the CRCP slab has a limited capacity of absorbing deformation (6.5 mm) due to its material properties. Few cracks have been found on the CRCP slab, but the width of cracks is large, and the internal force and anchor force are large. Through detailed performance comparison, the SHCC slab is more suitable for the performance requirements of the jointless bridge.

(4) The trilinear constitutive model based on the relationship between tensile strain and stress of the SHCC material prepared by experiment results is safe; the finite element package ABAQUS can be used to simulate the mechanical properties of an SHCC slab, and the calculation results are relatively safe.

The SHCC material could be successfully used in jointless bridge, but the cost is much higher than normal concrete. In the future, a more economical mix proportion will be found to lay the foundation for the wide use of this kind of jointless bridges.

Data Availability

The data used to support the findings of this study are included within the article.

Conflicts of Interest

The authors declare that they have no conflicts of interest.

Acknowledgments

This research was funded by Hunan Education Department Scientific Research Project, under grant nos. 16C1666 and 18C0291; also, this research was funded by the Central South University of Forestry and Technology College of Civil Engineering Youth Excellence Project, under grant no. 2017 YC0005.

References

[1] N. Ala, "Seamless bridge and roadway system for the U.S.practice," PhD Thesis, University of Nebraska, Civil Engineering, Lincoln, USA, 2011.

[2] M. Mojtaba and B. B. Jafar, "An investigation on the effect of cyclic displacement on the integral bridge abutment," *Journal of Civil Engineering and Management*, vol. 2, pp. 256–269, 2014.

[3] A. Sabe and A. R. Aleti, "Behavior of FRP link slabs in jointless bridge decks," *Advances in Civil Engineering*, vol. 2012, Article ID 452987, 9 pages, 2012.

[4] V. C. Mistry, *Integral Abutment and Jointless Bridges*, Federal highway administration, Washington, DC, USA, 2005.

[5] Y. B. Zhao, "Study on single expansion joint bridge applicable for large or medium bridge," PhD Thesis, Hunan University, Changsha, China, 2016.

[6] X. Jin, X. Shao, W. Peng, and B. Yan, "A new category of semi-integral abutment in China," *Structural Engineering International*, vol. 15, no. 3, pp. 186–188, 2005.

[7] X. F. Zhan, X. D Shao, and G. L. Liu, "Ductility performance analyses of the semi-integral jointless bridge," in *Proceedings*

of the 2014 Technical Congress on Resources Environment and Engineering, Hongkong, China, August 2014.

[8] X. F. Zhan and X. D. Shao, "Temperature effect of reinforced approach pavement of semi-integral abutment jointless bridge with pre-cutting cracks for temperature drops," *China Civil Engineering Journal*, vol. 44, no. 11, pp. 74–78, 2011.

[9] A. Gilani and P. Jansson, *Link Slabs for Simply Supported Bridges*, Michigan Department of Transportation, Lansing, MI, USA, 2004.

[10] M. Steffen and M. Viktor, "Use of strain-hardening cement-based composites(SHCC) in real scale Applications," in *Proceedings of the 4th International RILEM Conference on Strain-Hardening Cement-Based Composites(SHCC4)*, pp. 690–700, Germany, Europe, September 2017.

[11] Y. Y. Kim, G. Fischer, and V. C. Li, "Performance of bridge deck link slabs designed with ductile ECC," *Aci Structural Journal*, vol. 101, no. 6, pp. 792–801, 2004.

[12] V. C. Li, M. Lepech, and M. Li, *Field Demonstration of Durable Link Slabs for Jointless Bridge Decks Based on Strain-Hardening Cementitious Composites*, Michigan Department of Transportation, Michigan, USA, 2005.

[13] V. C. Li, G. Fischer, Y. Kim et al., *Durable Link Slabs for Jointless Bridge Decks Based on Strain-Hardening Cementitious Composites*, pp. 1–96, Michigan Department of Transportation, Michigan, USA, 2003.

[14] D. L. Michael and V. C. Li, "Application of ECC for bridge deck link slabs," *Materials and Structures*, vol. 42, pp. 1185–1195, 2009.

[15] N. Li, "*Performance of link slab using ECC and UHPC*," M.S. thesis, University of Maryland, College Park, MD, USA, 2019.

[16] V. C. Li, *Engineered Cementitious Composites (ECC)-material, Structural, and Durability Performance*, CRC Press: Publisher, Boca Raton, FL, USA, 2008.

[17] Z. G. Van and F. Wittmann, "Durability of strain-harding fibre-reinforced cement-based composites (SHCC)," *RILEM State of the Art Reports*, vol. 4, 2011.

[18] X. D. Shao, Z. X. Chen, X. Q. Jin et al., "Tensile deformation of reinforced approach pavement of jointless bridge," *China Journal of Highway and Transport*, vol. 23, no. 6, pp. 34–40, 2010.

[19] M. Mohamed and V. C. Li, "Flexural/tensile-strength ratio in engineering cementitious composites," *The Journal of Materials in Civil Engineering*, vol. 6, no. 4, pp. 513–528, 1994.

[20] V. C. Li and H. C. Wu, "Pseudo strain-hardening design in cementitious composites," in *High Performance Fiber Reinforced Cement Composites*, H. W. Reinhardt and A. E. Naaman, Eds., pp. 371–387, Springer, Berlin, Germany, 1992.